Turbulence

in shallow jet flows

By:
E.W.J. Bergsma
T. Bogaard

TU Delft
Delft University of Technology

Summary

The general flow pattern of an open channel flow, downstream of a width restriction by two artificial dams, is analysed. A physical Froude-scaled model, under hydraulic rough conditions, with a significant large Reynolds number is used to ensure turbulent flow.

Upstream of the dams the flow is uniform in transverse direction, in between and downstream of the narrow part a jet is formed. On both sides of the jet large eddies are formed bounded by the wall, the jet and the dams. Due to the large velocity gradient in transverse direction a mixing layer develops at both sides of the jet. The width of the mixing layer, as expected, grows with the downstream distance and exceeds the water depth. 2D structures are clearly visible by injecting dye. In the mixing layer besides the macro time and spatial scales, the small Taylor and Kolmogorov scales are present. Whereas the macro scales are well represented in the measured data, the small scales are impossible to mark due to limitations of the Doppler device.

When there is initial no net momentum in transverse direction present the jet is expected to appear symmetrical. However the jet is aligned to one of the sides every time the model starts to run. The preference for one or the other side seems to be random and cannot be related to momentum in transverse direction in between the dams. During measurements the position of the jet is stationary. The fixed position of the jet during measurements can be related to the Coandă effect.

When the flow is disturbed and transverse momentum is added to the upstream flow, the jet can be deflected. The position of the jet and the evolving mixing layers can be related very well to the measured velocities upstream.

Due to the limitations of the used momentum balance equation and use of the mean velocity in the bottom friction calculation the measured head loss is large compared to the calculated dissipative terms (bottom friction and Carnot loss).

Introduction

Today's developing populations require larger main ports all over the world. During the development and construction of these ports challenges arise. For example, the layout of harbour entrances in tidal areas can give rise to unwanted flow patterns. The main objective for the engineering company is to control the turbulent flow in such extent that unwanted flows and currents can be prevented.

To gather more knowledge about the behaviour of turbulent flows and the capability to control such a turbulent flow, Delft University of Technology wants to test the numerical outcome by a physical model. Thereupon this more general research project is started to analyse the turbulent flow in relative shallow water and flowing through two dams.

The research project is intended to be an exploration of the specific type of turbulent flows. Therefore the objective of this research project is to get more understanding an insight in asymmetric jet flows. Important is to get at first a clear qualitative view of the occurring flows and structures. From there on a quantitatively analysis can be executed.

The objectives and expectations of this research project are described in more detail in chapter one about the area of interest. Chapter two will portray the range of the physical setup to the data acquisition. Chapter three presents the experimental results including the velocity profiles. The quantitatively elaboration of the results is performed in chapter four where after in chapter five conclusions and recommendations will be presented.

Content

1 Main flow features

1.1 Objectives

When the width of an open channel is restricted, the streamlines converge at the upstream part of the flow. The flow velocities in stream wise direction are increasing. Far downstream where the channel width is as large as the upstream channel width, logically the stream wise velocity will be the restored towards a uniform pattern. However energy is lost due to bottom friction and from drag.

Shortly after the width restriction, the stream wise velocity is not uniform distributed over the cross profile. In the middle of the channel the velocities will be relatively large, near the wall there will be hardly any water movement at all.

One can expect a large velocity gradient over the cross profile. Expecting high velocities in the middle and low velocities near the wall. It is also possible that the large velocity gradient introduces instabilities. Eddies in all different length scales may be formed, covering a full turbulent flow regime.

The main objective is to give a description of the flow field directly downstream of the narrowing of the channel (in this case two identical dams, Figure 1-1). First a qualitative description and understanding of the general flow pattern is needed, focusing on the position of the jet and the large scale circulations.

Later on interesting parts of the flow field can be described quantitatively, by means of mean and fluctuating velocities.

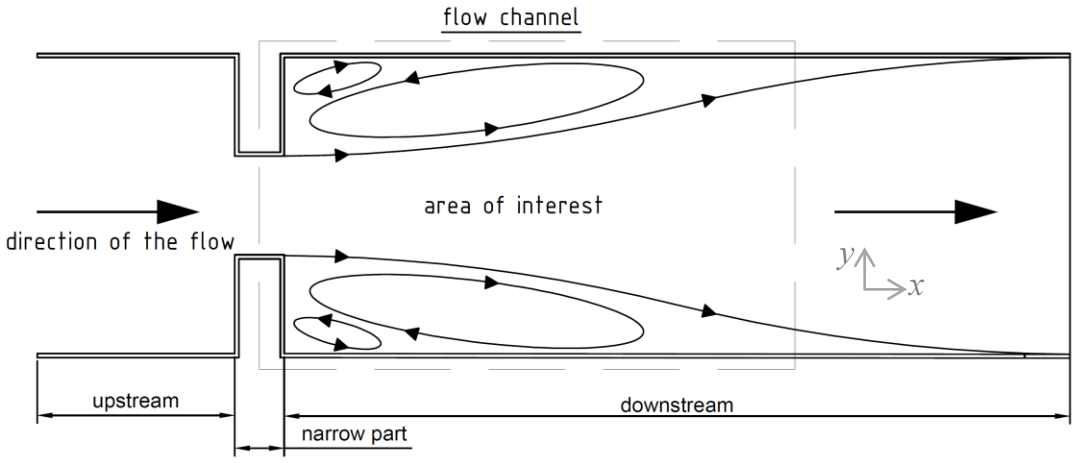

Figure 1-1 quantification of the area of interest

1.2 Expectations

1.2.1 General flow pattern

Downstream of the narrowed channel part one can expect a jet to be formed. The stream wise velocity in the narrow part will be relatively high with respect to the velocities in the wake zone of the dams. Where the streamlines upstream (of the narrow part) will be converging, after the dams they will diverge. Resulting in an increasing width of the jet and decreasing velocities along the mean flow direction. A stagnation point can be found at approximately eight times the length of the dam downstream. Assuming a symmetric situation (upstream flow pattern and channel geometry) we expect the flow field downstream to be symmetric as well, so a stagnation point can be found at both sides of the channel.

The water level at the stagnation point will be slightly higher than the water level near the dam. This water level gradient introduces a return flow along the walls of the channel. These large scale circulations are bounded by the dam and the position of the stagnation point in stream direction and by the wall and the jet in cross direction. Following the return

flow near the wall to the dam, streamlines have to deflect to the left. Since a right-angled streamline is impossible (causes infinitely high gradients), the streamlines are deflected smoothly to the left at some distance from the dam. This results in another circular motion bounded by the wall, the dam and the large scale circulation. Even though these "secondary" circular patterns are present they are hardly visible since the mean velocity in a circulation is in the order of 30 per cent of the driving flow.

1.2.2 Mixing layer

Because of the large velocity gradient in cross direction (high velocities in the center of the jet, low velocities in the recirculation zone) a substantial shear stress will be present between the two flow regimes. The large shear stress can cause instabilities; eddies of different sizes are spinning off. There is not one particular eddy length scale. There is a whole range of length scales present, from eddies with length scales of approximately the water depth (3D structures are bounded by the bottom and water level) to infinitely small whirls. The part of the flow where these instabilities arise is called the mixing layer. The mixing is in fact the part of the flow where the fluctuating velocities are large (order of 10% of mean flow velocity).

The width of the mixing layer generally grows in stream wise direction to a width of 20cm or more. It is also possible that 2D coherent structures introduce significantly larger length scales since their size is not bounded by the water depth.

1.2.3 Asymmetry of the flow

As mentioned above the geometry of the channel (including the narrow part) is symmetric. Therefore a symmetric flow pattern is expected. In practice, however, neither the geometry nor the flow pattern upstream will be exactly symmetric. Small deviations from a symmetric flow pattern upstream can lead to a asymmetric flow pattern downstream. The centre of the jet can deflect to a particular side of the channel depending on the upstream forcing.

When the upstream forcing is large enough the downstream flow pattern is influenced in such a way that the jet is attached to the wall. When this is the case, the jet will remain in this position by means of the Coandă effect. The turbulence in the mixing layer is entraining water next to the jet. At the wall there is supply to "entrain" energy from. There must be a significant upstream forcing in the opposite direction to change the position of the jet.

1.2.4 Energy dissipation

There are two main processes contributing to the dissipation of energy in the flow. The hydraulic rough conditions introduce a significant energy loss due to bottom friction. Also the turbulent motions, mainly present in the mixing layers, are dissipating energy. The energy dissipation introduced by bottom friction can be estimated by for instance the White-Colebrook formula, using flow and geometry parameters. The difference between the actual energy loss and the calculated dissipation of energy due to bottom friction is dissipated by turbulent motions. The energy dissipated by the turbulent motions can be roughly estimated by the Carnot equation, assuming momentum balance after the abrupt widening of the channel.

2 Methodology

In the previous chapter several objectives are determined whereupon questions arises about the translation into a model, numerical and/or physical. The known theory is not yet developed to such an extent that one is able to predict the entire turbulent flow. Most of the formulae consists of empirically determined parameters, that have little to do with the detailed physics.

Logically due to limitations in the theoretical description one is also not able to compute turbulent flows numerically. A big issue to compute the turbulent flows in a proper way is the insufficient computational power. This implicates that the smallest scales cannot be solved and an error is made, whether acceptable or not. In this case a numerical model is insufficient therefore a physical model is needed to gather more knowledge about this type of turbulent flows.

2.1 Physical model

2.1.1 The model geometry

At the laboratory of environmental fluid mechanics numerous flumes and facilities are available for research activities. In this case relatively shallow water is needed to simulate the real situation. Therefore the available 3 meter wide flume is used with a maximum water depth of 20cm.

The flume was adjusted to 2 meter in width by means of wooden sidewalls used in an earlier study. Approximately halfway the flume two identical dams are constructed perpendicular to the flow. Normally the bottom of the flume consists of glass but for this specific situation a rough bed is needed. Further details are discussed in the sections below.

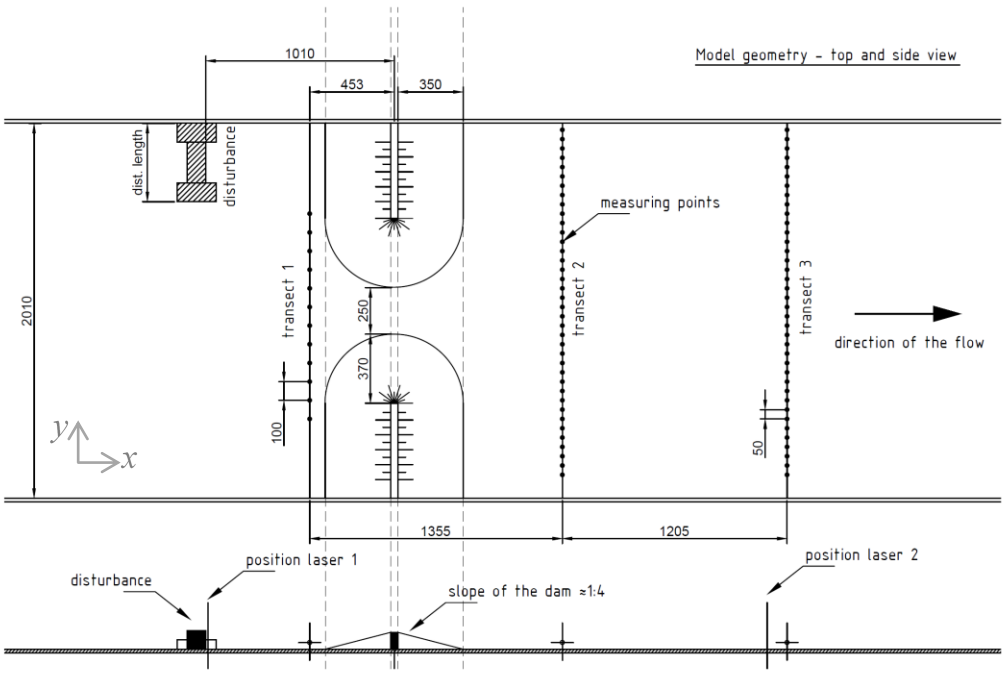

Figure 2-1 Model geometry

2.1.2 Height reference

In principal a clear reference level is needed to measure heights in a proper way. The glass bottom of the flume is assumed to be horizontal and the thin epoxy layer spread out. Therefore the top of the epoxy layer is used as being the reference level whereupon all height measurements are executed.

2.1.3 Coordinate system

Within the flume a coordinate system is defined. The positive x-axis is chosen to be in the streamwise direction. X equals zero is situated on the centreline of the disturbance in front of the two dams. If the flow is directed to the right in figures the axis should be rotated with an angle of $-\pi/2$ to get the positive y-axis. In all pictures a small indicator of the coordinate system is presented.

2.1.4 Scaling

In the upstream part of the flume a well-defined ideal flow has to be created in accordance with the study area. To control the flow the discharge can be adjusted and there is a possibility to change the height on the end of the flume to adjust the downstream depth.

Since it is not possible to create a physical model on real scale in the laboratory the model has to be scaled. In case of scaling two parameters are most important, the Froude number and the Reynolds number.

Froude number:

$$Fr = \frac{u}{c} = \frac{u}{\sqrt{gd}} \qquad \textit{Eq. 2-1}$$

Reynolds number:

$$\mathrm{Re} = \frac{\rho u l}{\eta} = \frac{ud}{\upsilon} \qquad \textit{Eq. 2-2}$$

In case of a free surface it is favourable to scale on the Froude number. This implicate that the Reynolds number should be high enough to create a turbulent flow anyway. A high enough Reynolds number is in the order of >4000.

In between the two dams the Froude and Reynolds numbers are roughly estimated for the parameters: U~0.3 m/s, d~0.07m, ϑ~1E-6 m^2/s,

Froude number:

$$Fr \approx \frac{0.3}{\sqrt{9.81*0.07}} \approx 0.362$$

Reynolds number:

$$\mathrm{Re} \approx \frac{0.3*0.07}{1*10^{-6}} \approx 21000$$

According to these values a discharge of 13.6 litres per second and a downstream water depth of around 9 centimetres is used in the experiments.

2.1.5 Hydraulically rough conditions

One can imagine that to approach the real situation the bed of the flume should be considered to be hydraulically rough. Accomplishing a hydraulically rough bottom, grains are glued to the glass plate. In order to determine if the applied grain size is large enough and for the computation of the bottom friction a grain size distribution is needed. This distribution is measured by hand and based on a 400 grains sample.

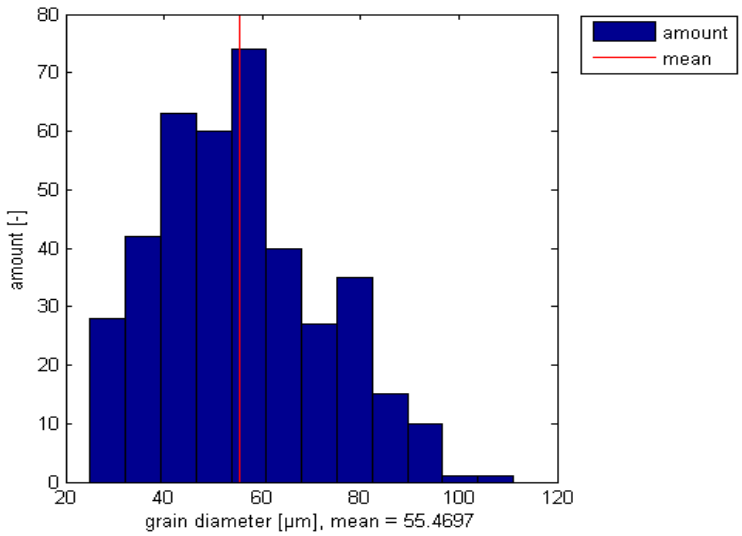

Figure 2-2 Grain size distribution

From this sampling can be deduced that the mean diameter is 55,47µm indicated by the red line in Figure 2-2. It should be mentioned that in this case only 400 samples are used and the uncertainty is unknown. Though it is possible to verify the grain size with a comparable earlier study (Ali & Uijttewaal, 2010) in the same flume where a grainsize range of 50µm - 80µm with a mean of 60µm is used. These values are in the same order of magnitude.

2.2 Equipment

2.2.1 Camera

Getting a qualitative understanding of the flume and its flows is essential. Therefore in first case different flow regimes are configured and captured with a camera. The camera is fixed with a tripod to the gantry crane of the laboratory right above the flume. To get a better view of the flow regimes small particles are dropped on the surface and potassium permanganate is injected in the streaming water.

2.2.2 Stagnation point device

Within different configurations, the stagnation point of the asymmetric jet changes. Tracking this change and to estimate the stagnation point relatively easy, a wooden bar with wool treads is attached to the glass plate on one of the sides of the flume. The wool treads indicate the stream direction upstream or downstream. If they are straight down the velocity is assumed to be zero and being an indication of the stagnation point.

2.2.3 Discharge measuring device

The discharge through the flume is adjustable with a valve at the water import pipeline. Controlling the discharge is executed by making use of a sonar discharge measurement device assembled to the pipeline. This device is measuring the discharge in litres per second. To gather proper data, the discharge should be between the limitations of the measuring device.

2.2.4 Height gauge

A very simple and acceptable accurate way of measuring heights is using a height gauge. With such a device it is possible to measure the heights with an accuracy of a 0.1mm.

2.2.5 Lasers

As described above, different configurations are used. To measure a change in heights of the free surface throughout the test of the configuration, lasers are assembled at fixed locations.

Calibration of the lasers is done in virtually still water, for which the free surface is horizontal. With the different configurations differences in heights are measured. These differences can be used to determine the energy loss due to turbulent flows and bottom friction.

2.2.6 Acoustic Doppler Velocimeter

Measuring velocities is done by using an acoustic Doppler velocimeter, in this case a Vectrino (NORTEK). The probe emits an acoustic signal and on approximately 5cm distance from the probe a sample volume is examined. The scattered and Doppler shifted signal is collected and transformed into velocities in x, y and z-direction.

For the proper scattering of the acoustic signal Chinese clay particles are injected into the streaming water.

2.3 Data acquisition

This section is especially about the measuring resolution and duration of the acoustic Doppler device. Other devices are less dependent on time and space intervals.

2.3.1 Resolution in time and space

Knowing at what time scale one is able to measure, is quite important regarding the limitations of the measurements. The acoustic Doppler that is used in this case has a maximum frequency of 25Hz. This frequency is used during the experiments.

Velocity measurements should be executed with certain intervals along a transect. To get a proper overview over the whole transect, spatial intervals of 5cm are used. Turbulence is proportional to gradients in velocities. In areas where a large gradient in velocities is observed a higher density of measurements is used. In order to gather more detailed information in the particularly areas a spatial interval of 2.5cm is applied.

The Doppler system creates a particular cylindrical sampling volume. The acoustic Doppler system automatically uses a fixed diameter of 6mm and the height of the cylinder can be adjusted. The applied height range of the sampling volume in the experiments is 2.5mm – 7.6mm depending on the strength of the signal.

2.3.2 Duration

Measuring velocities has to meet two duration requirements in general. The time interval should be short enough to consider the flow being stationary. The opposite is that the time interval should be large enough to get a representative picture of the flow. This includes also the relatively large scales of the flow regime. To meet these requirements a time interval of 5 minutes seems to be appropriate.

2.4 Configurations

As described in the section about expectations a symmetric jet flow in the middle of the flume is expected. However, the qualitative analysis of the flow already shows that the jet has a certain preference for one of the sides. An absolute preference is not observed, the side the jet chooses varies randomly.

Since the jet randomly abuts, it is decided to focus in this research on the "forced" flows with disturbances of the symmetry in front of the two identical dams. These disturbances consist of certain brick lengths perpendicular to the stream direction. To get a clear view on the influence of disturbances, different disturbance lengths are checked and a stagnation point analysis is executed.

2.4.1 Selection of configurations

As mention above briefly, the influence of different disturbance lengths is observed in relation to location of the stagnation point. The length of the disturbance is increased by brick lengths and gave the following results in relation to the stagnation point.

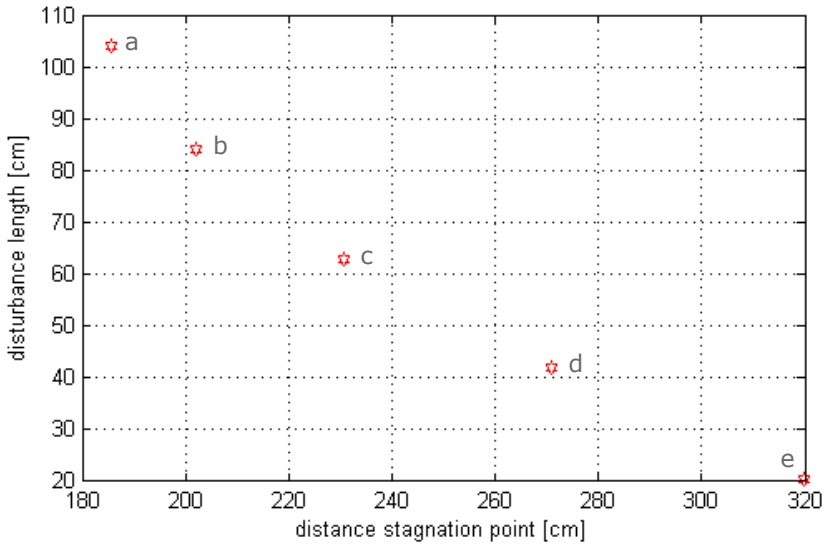

Figure 2-3 Relation increment of the disturbance and location stagnation point

Figure 2-3 indicates the decreasing influence of an equidistant increment of the disturbance length. Configurations representing point c and d are chosen as being 2 configurations. C and d are significant different from the initial situation without any disturbance and still have an adequate influence.

2.4.2 Configuration 1

The first configuration consists of a disturbance representing point c in Figure 2-3. This configuration is composed of a disturbance of three brick lengths placed perpendicular to the flow direction.

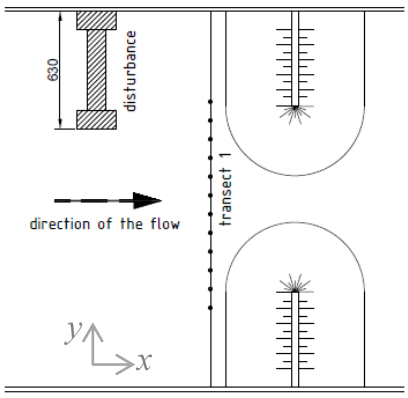

Figure 2-4 Configuration 1, top view

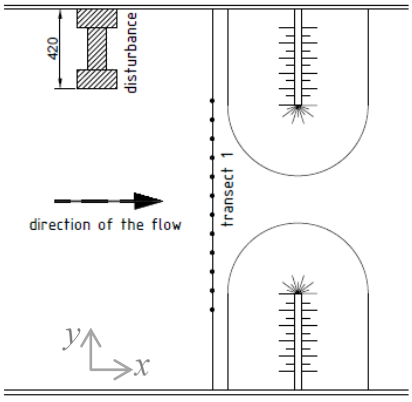

Figure 2-5 Configuration 2, top view

2.4.3 Configuration 2

The second configuration consists out of a disturbance representing point d in Figure 2-3. This configuration composed of a disturbance of two brick lengths placed perpendicular to the stream direction.

2.4.4 Configuration 3 and 4

Since the flow has a preference to abut to one of the sides, an initially forced configuration is introduced. The jet will be forced to one or the other side of the flume after which the disturbance will be removed. Therefore configuration 4 is a mirrored version of configuration 3.

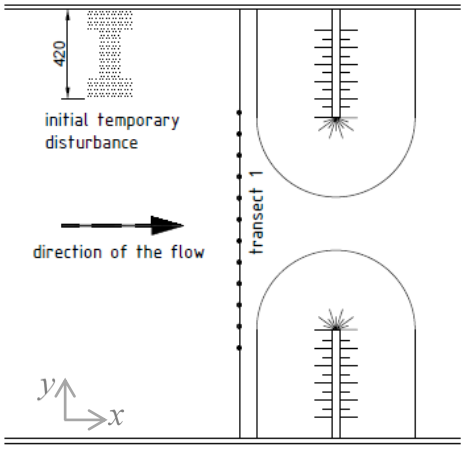

Figure 2-6 Configuration 3, top view

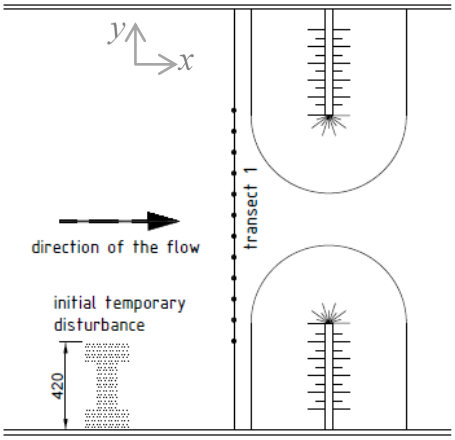

Figure 2-7 Configuration 4, top view

3 Experimental Results

3.1 General flow field

First we would like to understand the working of the flume and thereby observe the flow field qualitatively is essential. After that further analyses can be made. The general flow field and significant differences/similarities between configurations are described below.

3.1.1 Asymmetric outflow

Due to the upstream disturbance of the flow, an asymmetric inflow is observed as shown in Figure 3-1.

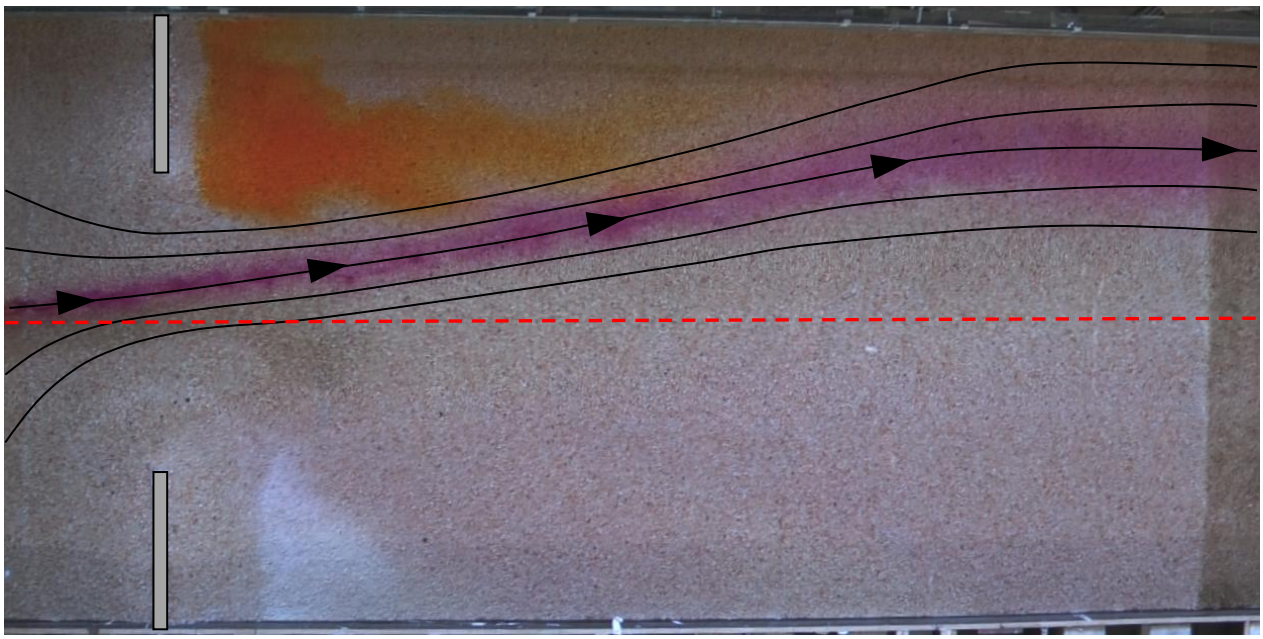

Figure 3-1 Overview of a asymmetric outflow, configuration 1

With all configurations an asymmetric outflow is observed. Though at configuration 3 and 4 an asymmetric outflow was not expected. Apparently the initial temporary forcing by the disturbance results in a persistent asymmetric outflow. This suggests that such a stable situation is a result of the so called Coandă effect.

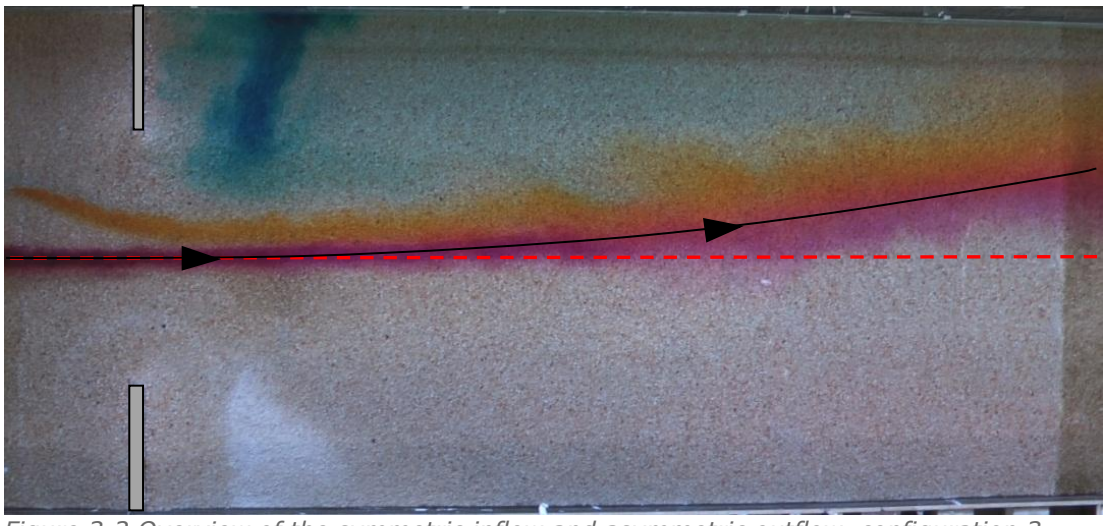

Figure 3-2 Overview of the symmetric inflow and asymmetric outflow, configuration 3

3.1.2 Recirculation cells

Due to velocity differences over the transect and resulting surface gradients, eddies and gyres develop next to the jet outflow. This eddies and gyres are named together as recirculation cells. The number and shape of the occurring cells is dependent on the upstream inflow. Within configuration 1, three primary circulation cells are observed as indicated in Figure 3-3. Apparently the recirculation cells split up if the disturbance length is increasing and the inflow has a greater angle. This phenomenon was observed with the determination of the relation between the increment of the disturbance and the location of the stagnation point.

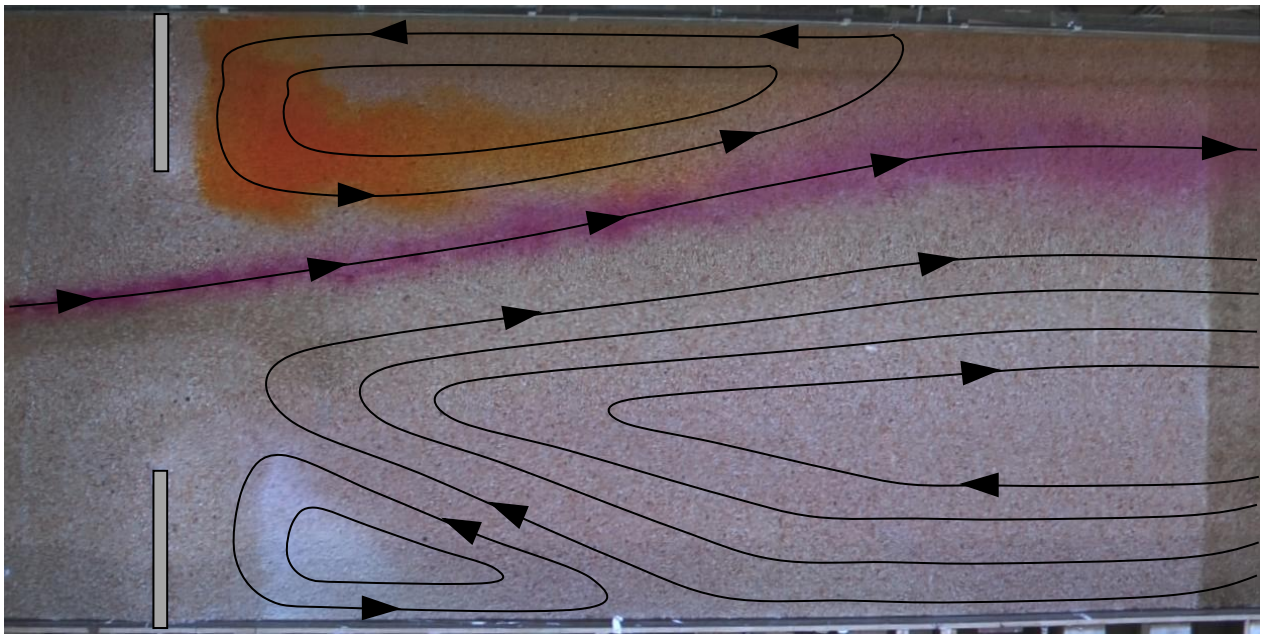

Figure 3-3 Recirculation cells in case of configuration 1

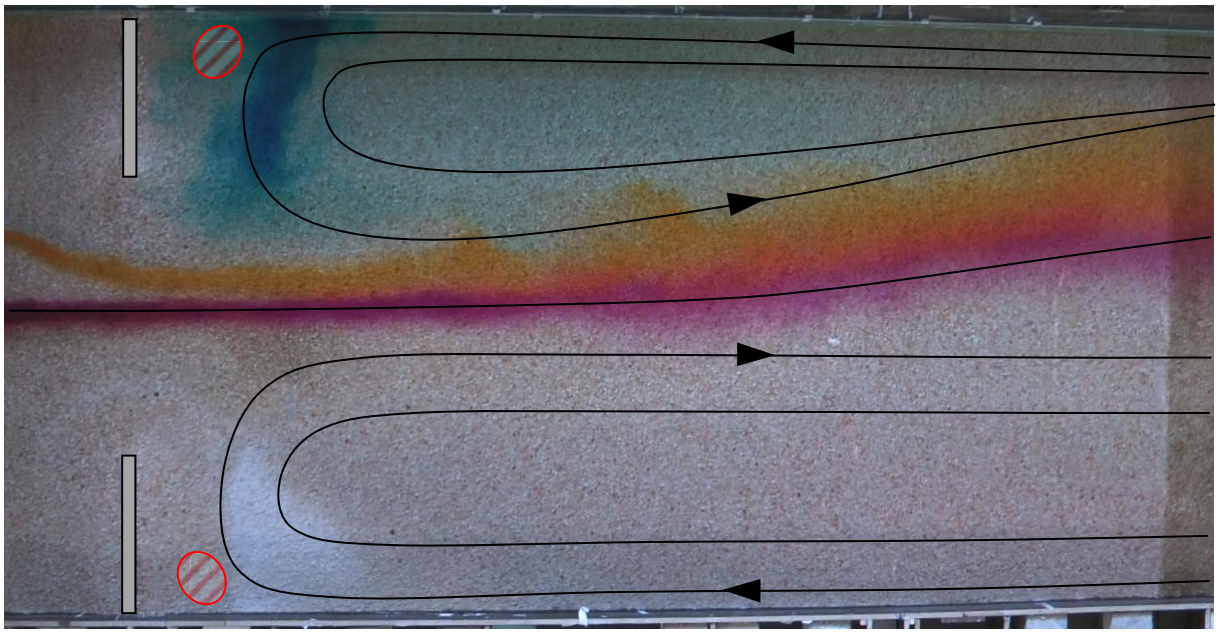

Figure 3-4 Recirculation cells in case of configuration 3

Figure 3-4 illustrates two relative large primary circulation cells as expected in chapter 1. Secondary relatively small circulations are observed and indicated by the red ellipses in Figure 3-4.

3.1.3 Interaction between jet and recirculation

To get a nice and clear overview of the turbulent flow different coloured dyes are used. Behind the two dams blending of the colours is observed. This blending is indicated by the hatched areas in Figure 3-5. This blending of colours denotes interaction between evolving flows, as expected in case of a turbulent flow.

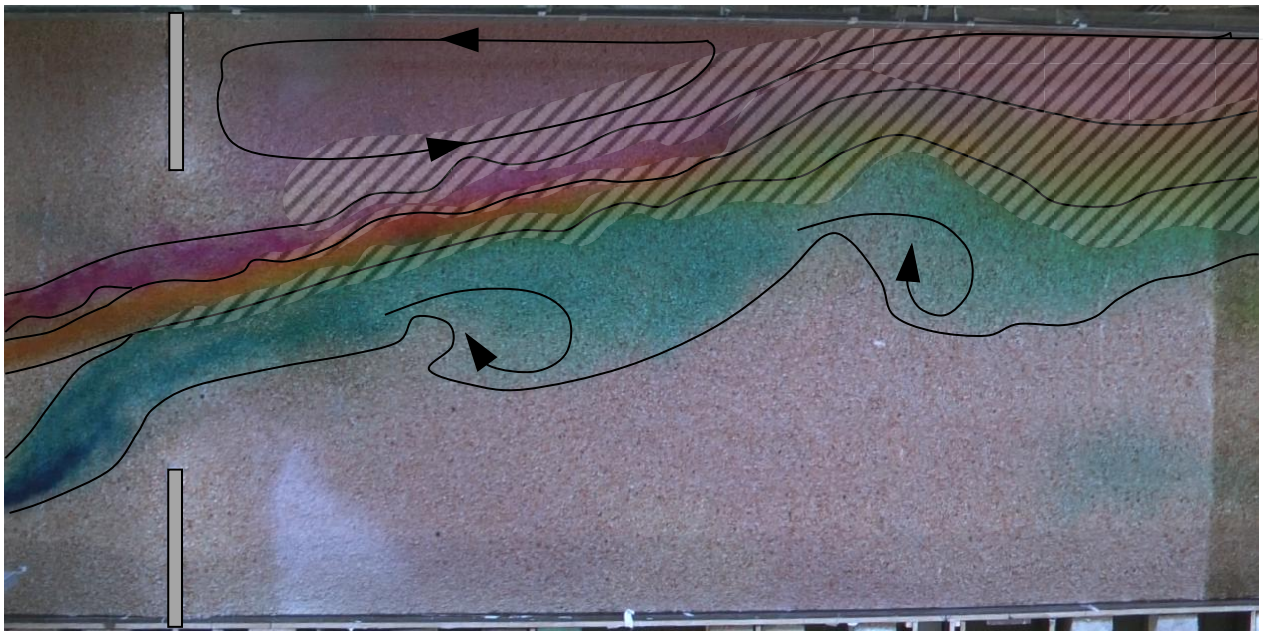

Figure 3-5 Interaction between flows, mixing layers

The recirculation zone in the north of Figure 3-5 shows an increasing concentration in time of the purple dye. Partially this is occurring due to turbulent interactions between the free shear flows in the so called mixing layer(Tennekes & Lumley, 1972). Another involved process is the separation of the dye containing flow at the stagnation point as shown below in Figure 3-6. In Figure 3-5 at the blue dye, two dimensional Kelvin-Helmholtz structures are observed, indicated with the bending arrows.

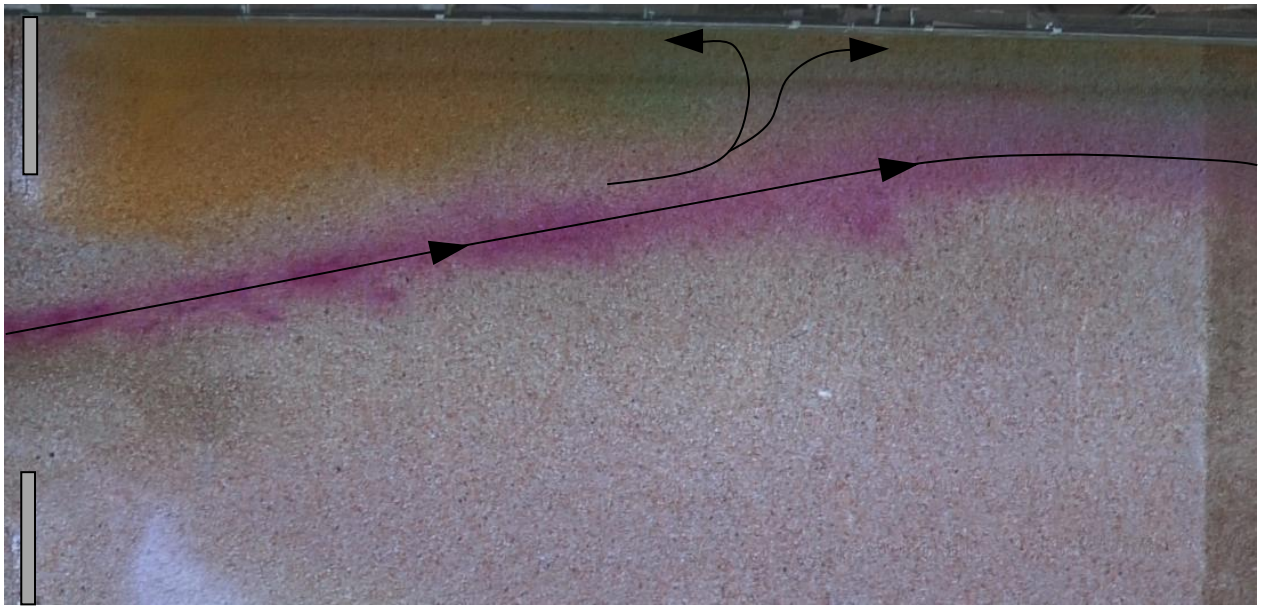

Figure 3-6 Separation of flows, visualized by the blending dye.

3.2 Velocity profiles

The raw data gathered by the acoustic Doppler is transferred into velocity profiles for further analysis. In general the velocity measurements are quite comparable to the expected values and the general flow field described above. All profiles can are presented in Appendix A: Velocity profiles.

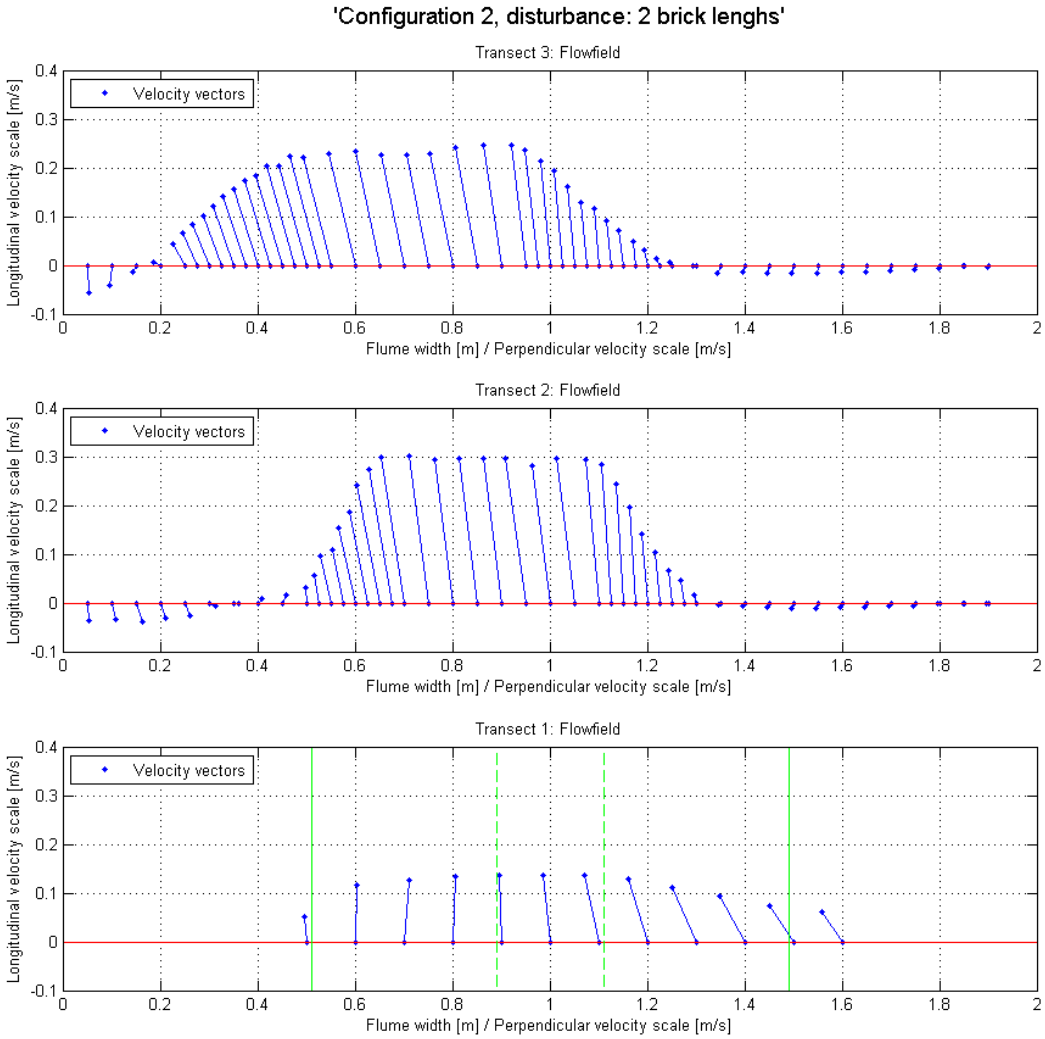

Figure 3-7 Velocity vectors per transect, configuration 2.

Figure 3-7 shows the first transect with an asymmetric flow in front of the two dams upstream. The green dashed lines indicate the width at the bottom and the solid lines indicate the crest of the dams. For this particular configuration the disturbance is located on the left side resulting in a left bend around the disturbance. At the transect, a left-hand directed velocity vector pattern is shown in accordance with visual observations.

Due to the disturbance upstream the jet outflow can be considered as being asymmetric as well. A result of the increasing disturbance length is an correlated increasing asymmetric outflow, see also Figure 2-3. This can be observed visually as shown in the section above. The velocity profiles of configuration 1 and 2 do confirm this hypothesis.

At first sight both downstream transects appear to be located within the area where the mixing layer is still developing by the evolving flow. This is indicated by the zero-gradient of the velocity in the centre of the jet (Tennekes & Lumley, 1972). At some point the mixing layers meet and the velocity at the jets centre will decrease. The distance x is in this case determined to be 6.41 times the characteristic width between the dams. Though the zero-gradient is present, the velocity in the centre of the jet is decreasing significantly. This energy loss can probably be ascribed to bed friction. Something which do not correspond to the theory described by Tennekes and Lumley(free flow).

3.2.1 Mirror effect configuration 3 & 4

Since configuration 3 and 4 are each other mirrors configuration, one would expect similar, but mirrored, flow fields and velocities. A close look to the upstream velocity profiles, in Figure 3-8 and Figure 3-9, does not confirm this hypothesis. The almost identical velocity profiles confirm the expectations of a symmetric upstream flow(no disturbance) but the vector in the centre is slightly deflected. This is remarkable since the initial temporary forcing is for each configuration on the other side. Apparently a different process is forcing both flows upstream in the same way slightly to the right.

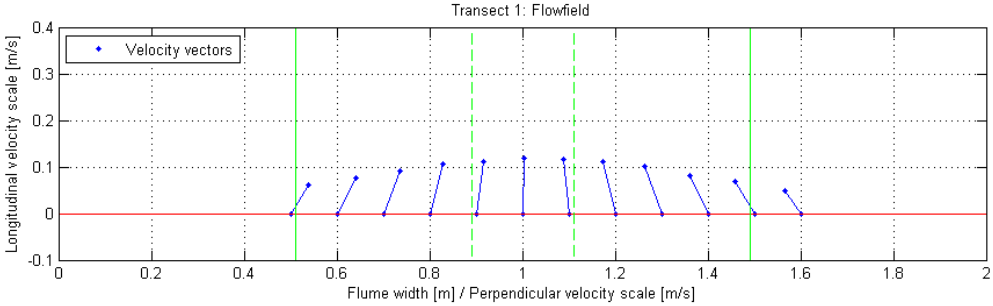

Figure 3-8 Configuration 3, velocity profile at transect 1

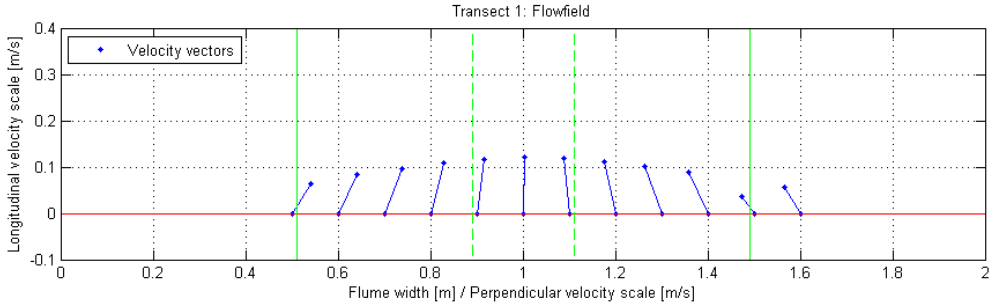

Figure 3-9 Configuration 4, velocity profile at transect 1

Though this inequality at the velocity profiles upstream, the downstream profiles show to be mirrored. These profiles are presented in Appendix A: Velocity profiles.

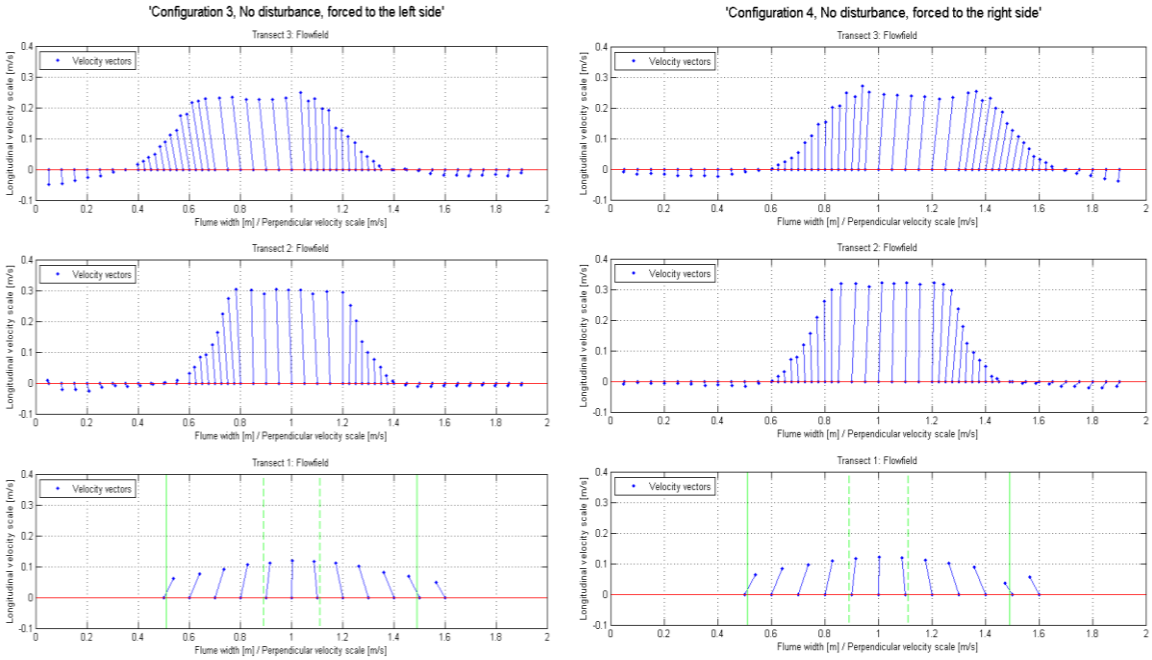

Figure 3-10 Configuration 3(left) and configuration 4(right)

3.2.2 Deflection capability

Referring to Figure 2-3, Figure 3-1 and Figure 3-2 one can observe significant differences between configurations. To some extent the figures show that one is able to affect the flow and thereby deflect the outflow into a certain direction. The velocity profiles confirm this statement, one can see that an increasing forced momentum results in an sharper angle of attack. The steering capabilities will be further discussed and quantified in chapter 4 .

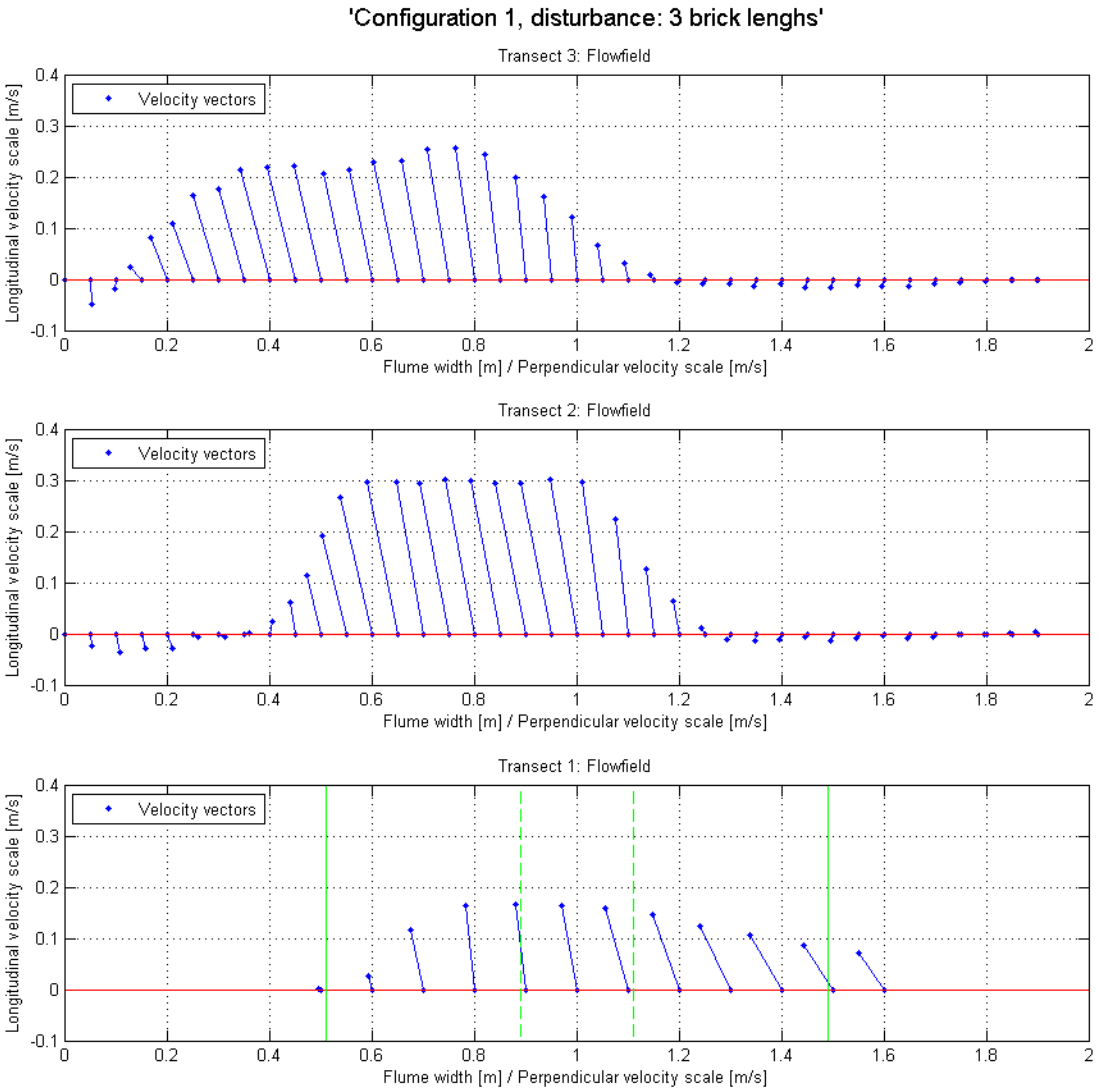

Figure 3-11 Velocity profiles configuration 1

4 Discussion

4.1 Development of the mixing layer

In general turbulence is produced in regions of high velocity gradients. This results in transport of mass and momentum thus defining a mixing layer. The development of this layer is of significant importance to general flow regime. Most of the literature describes the development of the mixing layer in case of a symmetric jet. In this section findings and possible approaches will be discussed to evaluate asymmetric flows.

4.1.1 Evolving flow

One of the main requisites for the development of turbulent flows is the presence of a velocity gradient. The differences in velocities in combination with turbulent fluctuations cause so-called Reynolds stresses. Since this turbulent fluctuations are proportional (around 10%) to the mean flow velocity, which remain constant(explanation below), the Reynolds stresses are expected to be in the same order of magnitude in every transection for a particular configuration.

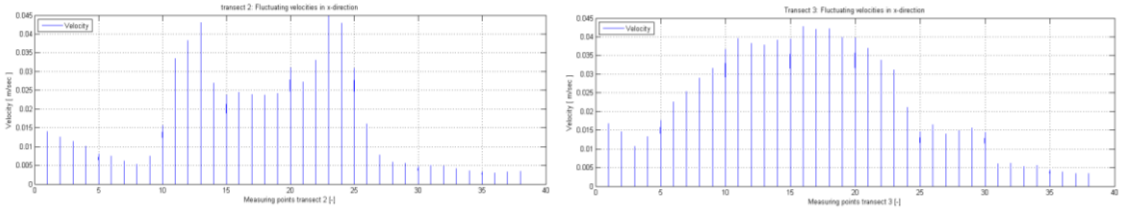

Figure 4-1 Fluctuating velocities in x-direction transect 2 and 3 of configuration 2

Since the velocity trough the gap between the dams is almost equal for all configurations the same order of magnitude is found for the different configurations.

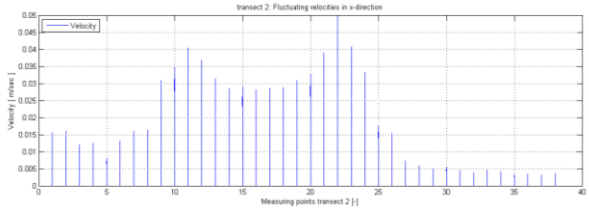

Figure 4-2 Fluctuating velocities in x-direction transect 2 of configuration 1

Besides the intensities of the turbulent fluctuations, a profound description of the growing mixing layer is favourable. An empirically relation is used that states $y = 0.078x$ (Tennekes & Lumley, 1972) to describe the boundaries of the mixing layer in case of a free flow. The averaged velocity in the jet remains constant. Like stated above this is not found in the research, probably due to bottom friction. Apparently the width of the mixing layer is linearly depending of the distance from the gap. In ratio to the characteristic width between the dams (D) the equation will be:

Ratio evolving mixing layer boundaries: $\frac{x}{D} = \frac{1}{0.078}$ *Eq. 4-1*

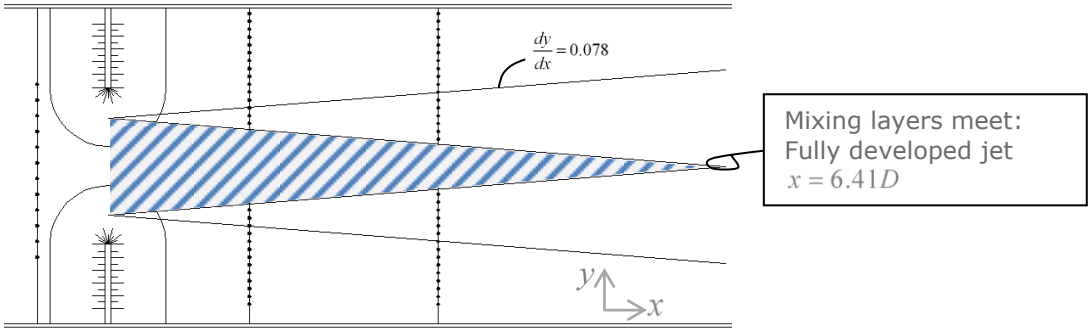

Figure 4-3 Top view of the development of the mixing layer.

To determine the needed length for the mixing layer to fully develop, the ratio is divided by 2 and becomes $\frac{dy}{dx} = 0.078$ as indicated in Figure 4-3. The hatched area in Figure 4-3 represents the area where the mixing layer is still developing. For $x > 6.41D$ holds that the turbulent flow becomes self-preserving.

Within the hatched area in Figure 4-3 the velocity gradient is assumed to be zero and equivalent to the velocity between the dams (Tennekes & Lumley, 1972). This implicates that according to this theory the velocity remains constant in the centre of the jet until the jet is fully developed. Over the mixing layer the velocity profile is fitted by a hyperbolic cosine (Tennekes & Lumley, 1972). Compared to the measured profiles this theoretical proposition is not entirely confirmed. The velocity in the centre of the jet seems to be decreasing over the length within the area where the mixing layer is still developing.

Since decreasing velocities are observed, the Reynolds stresses should also decrease. This holds since it is stated in the section above that the turbulent fluctuations and thereby the Reynolds stresses are proportional to the mean velocity.

4.1.2 Lateral shift

So far the development of a mixing layer can be described in case of a symmetric jet flow. For an asymmetric jet flow the transverse velocities can be considered as being most important. In Chapter 3 it was shown that an increasing asymmetric flow was found in case of an increasing disturbance length, which implicates an increasing y-directed velocity component and thereby of transverse nett momentum transport.

Coupling this momentum linearly to the deflecting effect of the mixing layer is briefly done by estimating the lateral shift:

Lateral shift: $$\Delta y = \frac{\Delta x}{\overline{u}} \overline{v} \qquad \text{Eq. 4-2}$$

The mean velocity ($\overline{v}$) in eq. 4-2 represents the width averaged velocity in y-direction between the dams. This velocity is derived from the measured velocities in transect 1. It is not possible to relate the velocities directly because transect 1 is positioned half a meter upstream of the dams and the flow is still converging at that point. In order to get a reasonable value for $\overline{v}$ in the calculations for configuration 1 and 2, the measured value of transect 1 is used which aligns to the middle of the gap between the dams. The used values for $\overline{v}$ in the symmetric configurations are close to zero and calculated by taking the mean of the velocities from transect 1.

The total description of the boundaries of the evolving mixing layer can be found by combining the development of the mixing layer in case of a symmetric flow and the lateral shift:

Mixing layer including shift: $$y = \left(\frac{\overline{v}}{\overline{u}} \pm 0.078 \right) x \qquad \text{Eq. 4-3}$$

Applying this straight forward approach results in a surprisingly close approximation to the measured mixing layers for configuration 1 and 2. Configuration 2 is shown in Figure 4-4.

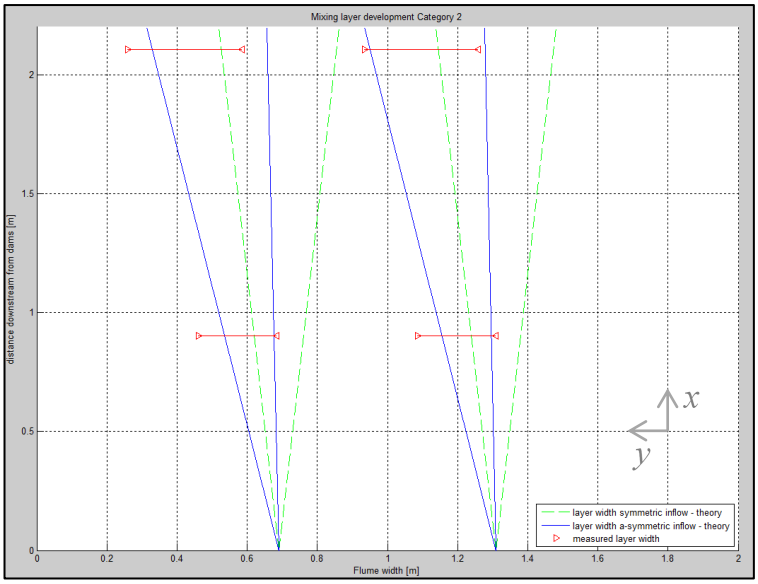

Figure 4-4 Mixing layer boundaries in case of a asymmetric flow, configuration 2

Configuration 3 and 4 give slightly different results as shown in Figure 4-5 for configuration 3. Comparison with Figure 3-2, with the dye representing the flow, gives a small amount of net y-momentum in front of the dams and a bending jet downstream. In chapter 3 it is described that the bending of the jet stream is due to the Coandă effect.

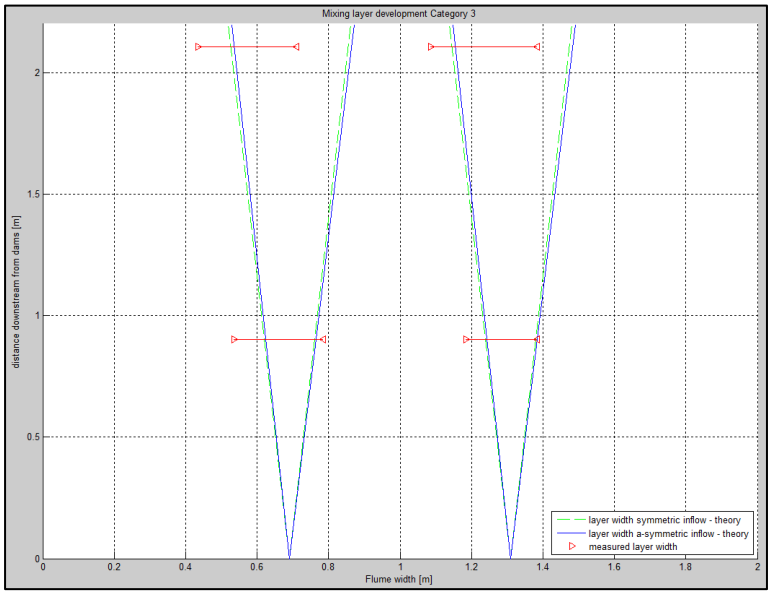

Figure 4-5 Mixing layer boundaries in case of a asymmetric flow, configuration 3

In case of the lateral shift approach the initial y-momentum will change the angle of attack of the mixing layer. In case of configuration 3 and 4, this implicates comparable mixing layers to a symmetric downstream configuration. Thereby the graph shows what to expect but does not meet the lateral shifting approach. One can reason about at what moment the initial y-momentum becomes more significant compared to the Coandă effect.

The horizontal red bars represent the measured mixing layers derived from the mean velocity profiles. Due to the spatial interval of 2.5cm between the measurements maximum error of the location and width is about 5cm. In all configurations a remarkable wider mixing layer is measured at transect 2.

4.1.3 Characteristic spatial and time scales

In order to describe the structure of the turbulent mixing layer the focus is on the different length and time scales that are present. The time scales can be extracted from the single point measurement in the mixing layer, by using the Taylor hypothesis. Relating the turbulent time scales to the length scales by the mean velocity in the mixing layer (Tennekes & Lumley, 1972).

Turbulent time scale:

$$T_t = \frac{L}{u} \qquad \text{Eq. 4-4}$$

The autocorrelation function of the fluctuating velocities represents in principle two time scales, the micro(Taylor) and macro time scales. The taylor time scale is hardly visible because the spatial scale is of the order of the width of the measuring volume (acoustic Doppler).

Taylor time scale:

$$\frac{\lambda_{tay}}{l} = \left(\frac{15}{A}\right)^{1/2}\left(\frac{ul}{\upsilon}\right)^{-1/2} = \left(\frac{15}{A}\right)^{1/2} R_l^{-1/2} \qquad \textit{Eq. 4-5}$$

Where: $u^2 \sim \overline{u'v'}$; $A \cong 1$ and $l \sim \frac{1}{2} \times width\ of\ the\ mixing\ layer$

Substituting for example the values for the mixing layer in configuration 2, transect 2:

Taylor time scale:

$$\lambda_{tay} = \left(\frac{15}{1}\right)^{1/2}\left(\frac{\sqrt{0.02*0.04}\times\frac{1}{2}\times 0.141}{1\times 10^{-6}}\right)\times\frac{1}{2}\times 0.141 \simeq 0.005m$$

The width of the measuring volume varies between 2.5 and 7.6 mm, while the height is 6mm. The spatial macro scale is expected to be in order of the mixing layer width. In the table below the expected macro spatial scale based on the mixing layer width according to the theory described above is compared to the scale extracted from the autocorrelation function (the autocorrelation is computed between the fluctuating velocities in y-direction). For transect 2 the autocorrelation nicely represents macro time scales (see figure below – autocorrelation configuration 1, transect 2). For transect 3 the autocorrelation is not that clear, so the focus will be on transect 2. The energy density spectrum contains in fact the same information as the autocorrelation function and is presented in Appendix B: Power density spectrum .

		Meas. point	$\overline{u_{mixing\ layer}}$ [m/s]	$L_{t,theory}$ [m]	$L_{t,measured}$ [s]	$T_{t,v}$ [s]
Config. 1	Trans. 2	11	0.1908	0.141	0.67	3.5
Config. 1	Trans. 3	7	0.1767	0.329	*0.88*	*5 and >14*
Config. 2	Trans. 2	13	0.2412	0.141	0.77	3.2
Config. 2	Trans. 3	22	0.1159	0.329	*0.27*	*2.3*

Table 1 Characteristic time and spatial scales of configuration 1 and 2.

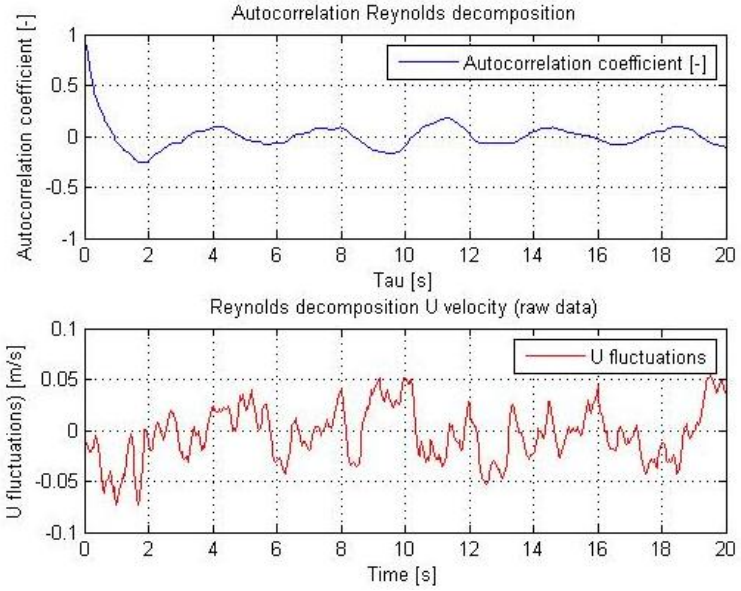

Figure 4-6 Graph above: Autocorrelation function of fluctuating velocities in y-direction, configuration 1, transect 2, in mixing layer. Graph below: part of the raw data of the fluctuating velocities in y-direction at the same position.

Compared to the expected macro scale, the scale showed by the correlation functions is rather large. The Coherent structures that are appearing seems to be two dimensional (since the water depth is in the order of 0.1m) and have to be interpreted as Kelvin-Helmholtz instabilities (Prooijen & Uijttewaal, 2002).

4.2 Head loss

According to paragraph 1.2.4 we expect two major sources of energy loss in the area downstream the dams: bottom friction and energy loss due to turbulent motions. In this paragraph the different sources will be quantified in the area from the dams till the flow has become uniform again.

4.2.1 Energy balance

To calculate the mean (depth and width averaged) velocity in x-direction between the dams an energy balance is used. The system of equations to solve contains the straightforward Bernoulli and continuity equation and an equation for the equivalent width in between the dams (due to the slope of the dams the width is not known in advanced).

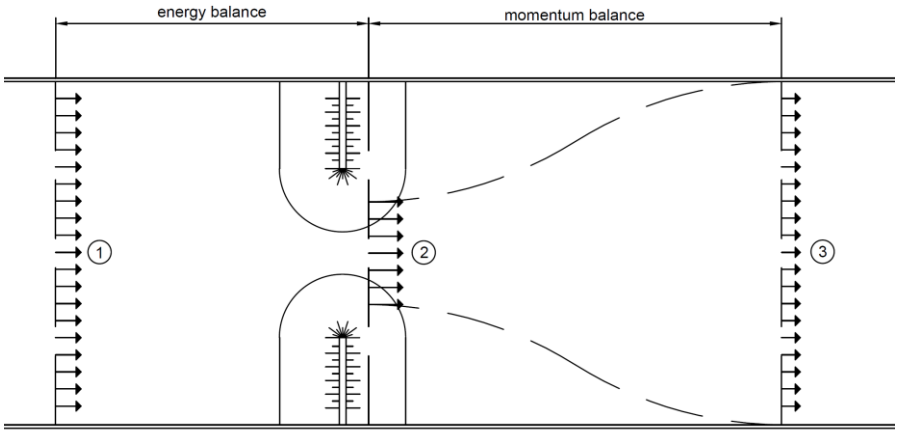

Figure 4-7 Overview energy balance (1-2) and Momentum balance (2-3)

Bernoulli:

$$h_1 + \frac{u_1^2}{2g} = h_2 + \frac{u_2^2}{2g} \qquad \text{Eq. 4-6}$$

Continuity: $$b_1 h_1 u_1 = \alpha b_2 h_2 u_2$$ *Eq. 4-7*

Equivalent width: $$b_2 = b_{bottom} + \frac{h_2}{\beta_{slope}}$$ *Eq. 4-8*

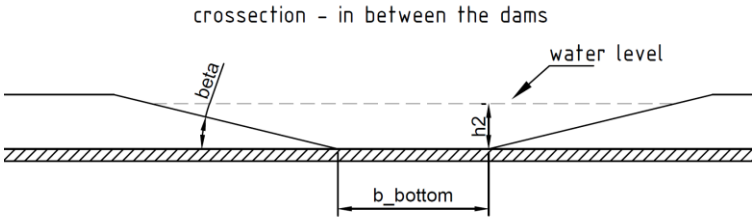

Figure 4-8 Equivalent width, parameters

The solution of the system is tabled below.

Parameters – energy balance					
Upstream conditions			Conditions between dams		
h_1	0.0965	M	h_2	0.0923	m
u_1	0.071	m/s	u_2	0.28	m/s
b_1	2.01	m	b_2	0.61	m
α	0.85	-			
β_{slope}	350/90	-			
b_{bottom}	0.25	m			

Table 2 Energy balance parameters

According to the theory described in paragraph 4.1.1 the mean velocity between the dams (in the center of the jet) equals the mean velocity in the center of the jet at transect 2 and 3. The calculated (depth and width averaged for a uniform stationary flow, with an alpha value of 1) velocity however is rather small compared to the measured mean velocities in transect 2. A reason for the differences in measurements and calculation can be the influence of the geometry of the wet area between the dams. A contraction coefficient should be taken into account to take care of the geometry influence. A reasonable contraction coefficient of 0.85 results in mean velocities of 0.28 m/s, which are comparable to the measured values. In addition the measurements show a velocity decrease between transect 2 and 3. This decrease however cannot be explained by a contraction coefficient. Since the used theory describes a fully free jet and the development of the jet flow in this particular situation is influenced by the wall, a reason for this velocity decrease can be bottom friction.

4.2.2 Carnot loss

A momentum balance is used to calculate the Carnot loss (see fig. 4.7). The set of equations to solve contains of the continuity equation, a hydrostatic pressure expression and the momentum balance between the boundaries of the described area.

Hydrostatic pressure location 1: $$p_2 = \frac{1}{2}\rho g h_2$$ *Eq. 4-9*

Hydrostatic pressure location 2: $$p_3 = \frac{1}{2}\rho g h_3$$ *Eq. 4-10*

Continuity: $$\alpha b_2 h_2 u_2 = b_3 h_3 u_3$$ *Eq. 4-11*

Momentum balance: $\Delta p = \rho u_3 \left(u_2 - u_3\right)$ *Eq. 4-12*

Finally the Carnot loss is calculated by substituting the mean flow velocities in the following equation:

Carnot loss $\Delta_{h,carnot} = \frac{\left(u_2 - u_3\right)^2}{2g}$ *Eq. 4-13*

Quantitatively, $\Delta_{h,carnot} = \frac{\left(0.28 - 0.070\right)^2}{2 \times 9.81} = 0.002m$

4.2.3 Bottom friction

Bottom friction can be calculated with different approaches. However, bottom friction is highly dependent on the flow velocity and high velocities do have a relative large contribution to friction loss. To account for the different velocities, an estimation is made between the different points. The velocity is assumed to behave linearly (see Figure 4-9).

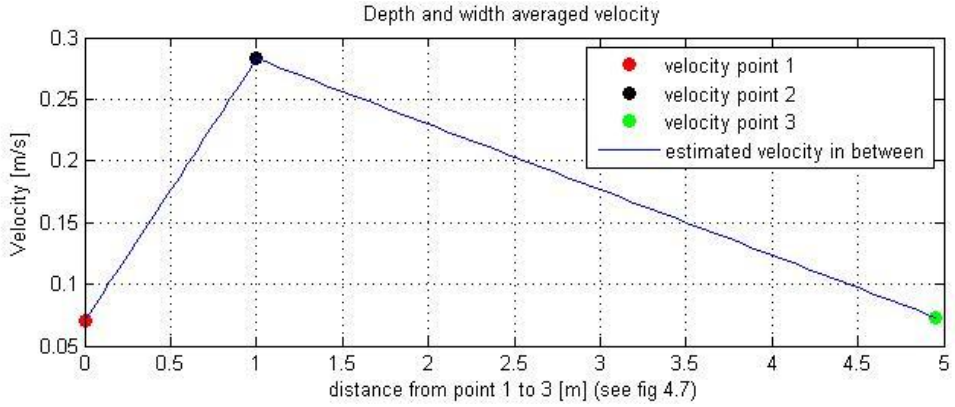

Figure 4-9 Estimation of depth and width averaged velocities

At the third point (where the velocity is the lowest) a Reynolds number of 62000 is found (in case of L=R) with equation 2-2. The Reynolds number is sufficiently larger than 4000, which implicates a turbulent flow and the applicability of the White-Colebrook equations, (Battjes, 2002).

White-Colebrook: $\frac{1}{\sqrt{f}} = 2\log\left(\frac{3,7R}{k\left(1+3,3/\mathrm{Re}_*\right)}\right)$ *Eq. 4-14*

There is no clear explicit value for k, several are known to determine a proper value. In this case k is determined to be $3.5D_g$ representing 3.5 times the mean grain size. The formula of White-Colebrook gives the following results:

Parameters	Value	Dimension
Re_*	870.62	[-]
c_f	0.004	[-]
$\Delta_{h,\,friction}$	4.91E-05	[m]

Table 3 Computed frictional parameters

4.2.4 Measured head loss

The total energy level consists of a static (water level) and a dynamic (kinetic energy) part. In paragraph 4.2 the water level and flow velocity (between the dams) is calculated. With the measured water level downstream and the continuity equation (inflow equals outflow) the total measured head loss can be calculated. The total head loss is in the order of $\Delta_{h,measured} = 0.0025m$ [1].

4.2.5 Comparison measured and calculated head loss

In principle the energy loss due to bottom friction and the Carnot loss (turbulent motions are in fact responsible for the Carnot loss) sum up to the measured head loss. The actual head loss however appears to be larger than the calculated value. The difference between the two can be explained by the simplification of the momentum balance (Carnot-equation neglects the wall friction and the velocity of the large eddies) and the used mean velocity for the bottom friction calculation. The large velocities have a relatively high contribution to the bottom friction term. By using the mean velocity the loss due to bottom friction is underestimated.

$$\Delta_{h,measured} = 2.5\times10^{-3}m$$

$$\Delta_{h,carnot} + \Delta_{h,\,friction} = 4.9\times10^{-5} + 2.0\times10^{-3} = 2.05\times10^{-3}m$$

The table below gives the relative contributions of the different dissipative terms (calculated values as percentage of the measured head loss).

Bottom Friction	2	% of measured head loss
Carnot Loss	80	

Table 4 Percentages of total measured energy dissipation

[1] There is a relative wide range at which the measured water level data from the height gauge is varying (0.003 mm). And since there water level is measured with only two different lasers downstream the data from the different instruments is hardly comparable.

5 Conclusions and recommendations

5.1 Conclusions

5.1.1 General flow field

The general flow field met the expectations quite well. As described a jet was formed downstream the dams and recirculation cells were also observed. When the flow field is symmetric, a stagnation point (on both sides of the flume) is expected at a downstream distance of approximately eight times the length of the dam. Since the hydraulic rough bed was not extended to this downstream distance the stagnation points were not observed in symmetrical situations. When the jet is more and more deflected to the wall, the stagnation point shifts towards the dam (at the side of the channel at which the jet is deflected). The shifting can be related properly to the upstream forcing of the jet.
The large recirculation cells are present on both sides of the jet. When the flow is asymmetric and the jet deflects, the velocities in the recirculation cell at the side to which the jet deflects met the expectations (30% of the velocity in the jet). The velocities in the recirculation cell at the other side are significantly smaller.
Secondary recirculation cells (with velocities in the order of 30% of the velocity in the major recirculation cell) are observed in asymmetrical situations, located near the recirculation cell with the highest velocity.

In symmetrical situations, with no significant transverse velocities upstream, the jet and the mixing layers are expected to appear symmetrical. Even when there was no initial forcing the jet deflects to one of the sides randomly, resulting in an asymmetrical flow pattern. Once the jet was aligned to a particular side it stays in this position. This phenomenon is known as the Coandă effect. The deflection of the jet in undisturbed (no forcing upstream) situations cannot be related to the presence of net momentum in transverse direction upstream.

When the jet is aligned to one or the other side one can influence the position of the jet by introducing a forcing upstream (increasing the cross-velocities in the direction opposite to the alignment of the jet). When the forcing is large enough the jet loses contact with the wall and deflects to the other side.

5.1.2 Mixing layer

Due to the large velocity difference between the jet flow and the recirculation cells, large shear stresses results in two evolving mixing layers. The fluctuating velocities in the mixing layers are in the order of 10% of the mean flow component.
In the mixing layer friction induced eddies and whirls of all sizes (from Kolmogorov scale to eddies, bounded by the water depth) are present in all three directions. In the horizontal plane 2D structures much larger than the water depth are observed. The 2D coherent structures are clearly visible by injecting dye and can be quantified by means of the autocorrelation or spectral analysis of the measured data. The Kolmogorov and even the Taylor time and spatial scales cannot be measured with the acoustic Doppler device.

During the experiments with a forced upstream flow, the lateral shift of the mixing layer can be related properly to the transverse flow velocities upstream.
The growth of the mixing layer width is proportional to the downstream distance of the dams and the width of the layer becomes eventually larger than the water depth, which indicates the presence of 2D structures.

5.1.3 Head loss

The measured head loss seems to be larger than the calculated loss (bottom friction and Carnot loss). The difference can be explained by the simplification of the momentum balance and the used mean velocity for the bottom friction calculation. Since there are still negative velocities (introduced by the recirculation cells) at the boundary of the balance domain, the applied momentum balance does not fully represent the actual situation.

By using a mean velocity for the bottom friction calculation, one underestimates the contribution of the relative high velocities since the bottom friction is not linear dependent upon the flow velocity.

5.2 Recommendations on measurements and methodology

- In order to quantify the asymmetry of the flow it is recommended to determine the locations of the stagnation points on both sides of the flume. Another device must be used to define the location of the stagnation points when the same velocities are used in future experiments. When the velocities in the recirculation cells are small, the woollen threads are insufficient.

- When a similar set-up is used for further research it will be useful to measure the velocities directly in between the dams. During the experiments the velocities were measured approximately a half a meter upstream of the dams, calculations had to be made to come up with the velocities between the dams.

- When there is no forcing upstream and the jet is attached to the wall, one can introduce forcing by increasing the velocity in transverse direction. To quantify the strength of the Coandă effect one can measure the transverse momentum upstream at the critical moment the jet is changing his position.

- Since the contribution of bottom friction to the head loss is difficult to calculate properly (the roughness height is highly arbitrary) it is recommended to do measurements with the laser devices in a uniform flow in order to come up with a measured head loss. One can also vary the parameters water height and discharge and eventually compare the results for different situations.

- During the velocity measurements the data collection time was set up to 300 seconds. Since the autocorrelation approaches zero after a maximum of four seconds the collection time is rather large. To get reliable averages a collection time of 80 seconds should be sufficient.

- The water heights are measured by a height gauge and at two downstream positions by a laser device. The rough bed and ripples in the free surface causes difficulties when using the height gauge. In order to get more reliable results one should use more laser devices.

- The rough bed should be enlarged further downstream in order to measure the stagnation points at both sides of the flume. The rough bed should be extended to approximately ten times the length of the dam.

References

Ali, S., & Uijttewaal, W. (2010). Flow resistance due to vegetated weir-like obstacles during high water stages. Proceedings of river flow. Brauschweigh, Germany.

Battjes, J. (2002). *Vloeistofmechanica (Lecture notes).* Delft, The Netherlands: Delft University of Technology.

Jirka, G. (sd). *Large scale flow structures and mixing processes in shallow flows.* Karlsruhe, Germany: Institute for Hydromechanics, University of Karlruhe.

Kantoush, S., & Schleiss, A. (2009). Large-Scale PIV Surface Flow Measurements in Shallow Basins with Different Geometries. *Journal of Visualization, Vol 12, No.4*, 361-373.

Prooijen, B., & Uijttewaal, W. (2002). A linear approach for the evolution of coherent structures in shallow mixing layers. *Physics of fluids, Vol 14, No.12*.

Tennekes, H., & Lumley, J. (1972). *A First Course in Turbulence.* Massachusetts: The Massachusetts Institute of Technology.

List of symbols

δ	=	Thickness of the boundary layer
λ_{tay}	=	Taylor time scale
η	=	Viscosity
ρ	=	Density
τ	=	Shear stress
υ	=	Kinematic viscosity
A	=	Scale factor (used in the Taylor time scale formula)
c	=	propagation
c_f	=	Friction factor
D	=	Width between the dams
D_g	=	Grainsize diameter
f	=	Friction coefficient
Fr	=	Froude Number
g	=	Gravity
k	=	Skin resistance coefficient
L	=	Length scale
R	=	Hydraulic radius
Re	=	Reynolds Number
u	=	Velocity in x-direction
u'	=	Velocity fluctuations in x-direction
$\bar{u}$	=	Average velocity in x-direction
u_*	=	Shear stress velocity
v	=	Velocity in y-direction
v'	=	Velocity fluctuations in y-direction
$\bar{v}$	=	Average velocity in y-direction

Appendices

Appendix A: Velocity profiles

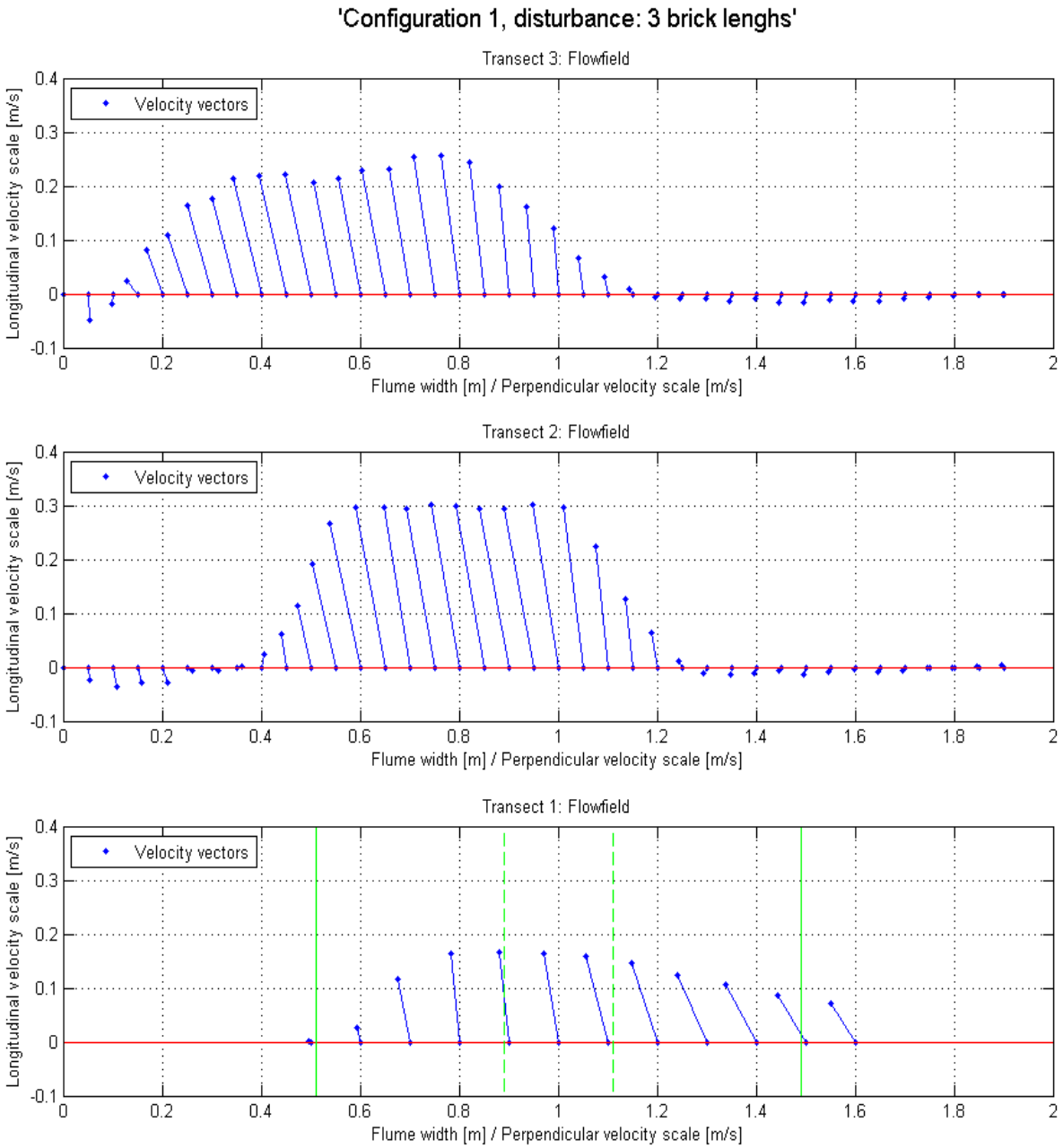

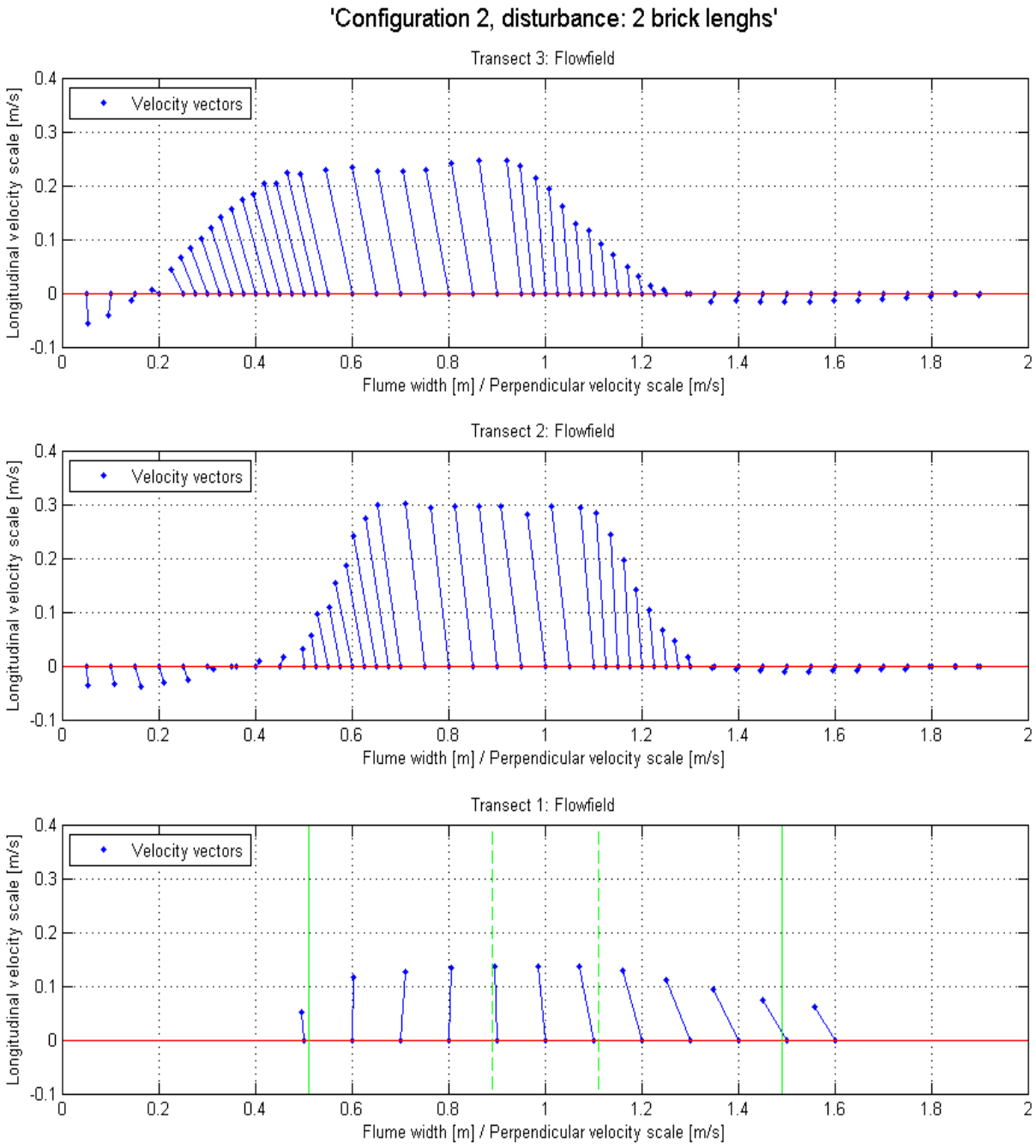
'Configuration 2, disturbance: 2 brick lenghs'
Transect 3: Flowfield
Velocity vectors
Longitudinal velocity scale [m/s]
Flume width [m] / Perpendicular velocity scale [m/s]
Transect 2: Flowfield
Velocity vectors
Longitudinal velocity scale [m/s]
Flume width [m] / Perpendicular velocity scale [m/s]
Transect 1: Flowfield
Velocity vectors
Longitudinal velocity scale [m/s]
Flume width [m] / Perpendicular velocity scale [m/s]

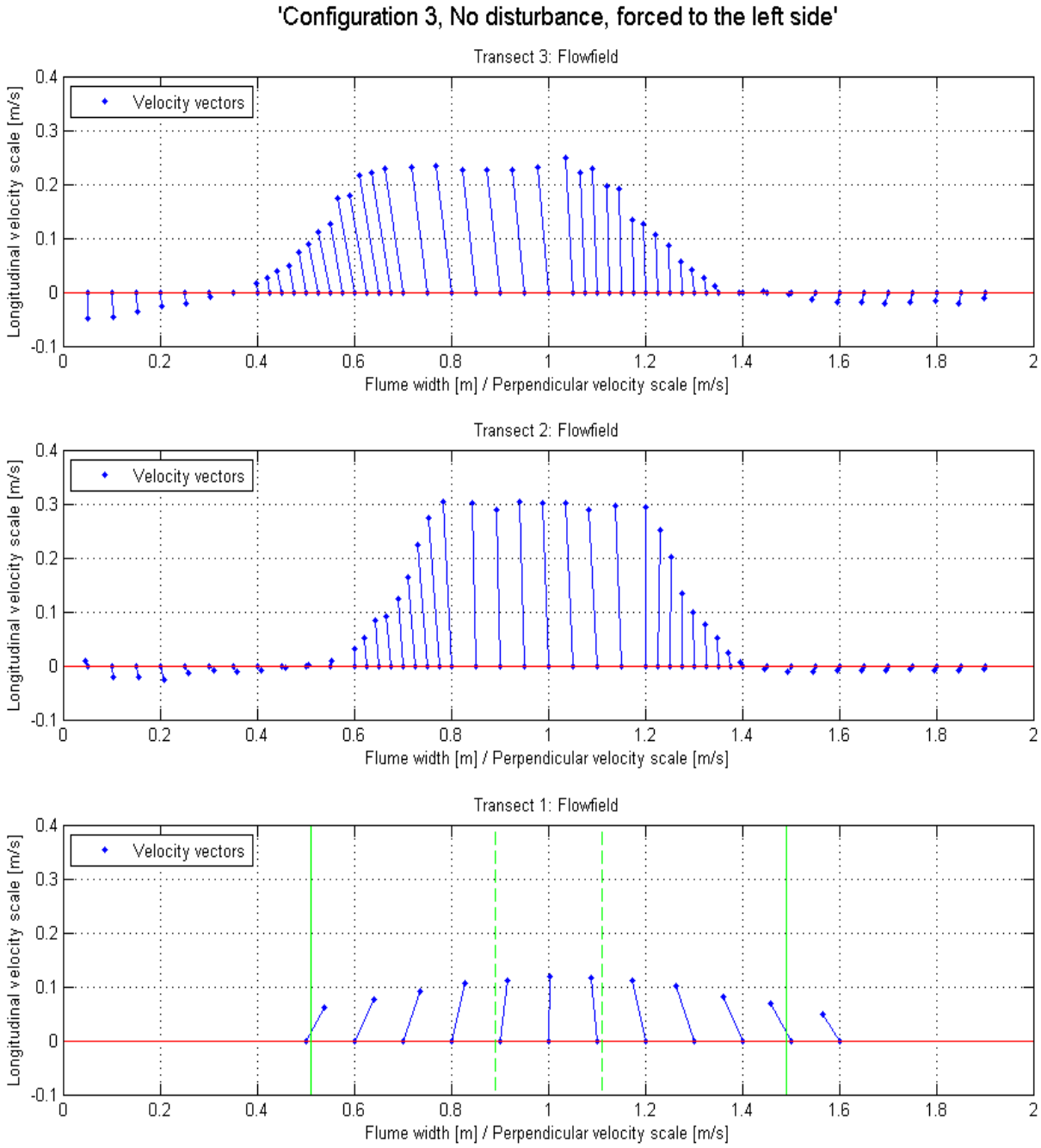
'Configuration 3, No disturbance, forced to the left side'
Transect 3: Flowfield
Velocity vectors
Longitudinal velocity scale [m/s]
Flume width [m] / Perpendicular velocity scale [m/s]
Transect 2: Flowfield
Velocity vectors
Longitudinal velocity scale [m/s]
Flume width [m] / Perpendicular velocity scale [m/s]
Transect 1: Flowfield
Velocity vectors
Longitudinal velocity scale [m/s]
Flume width [m] / Perpendicular velocity scale [m/s]

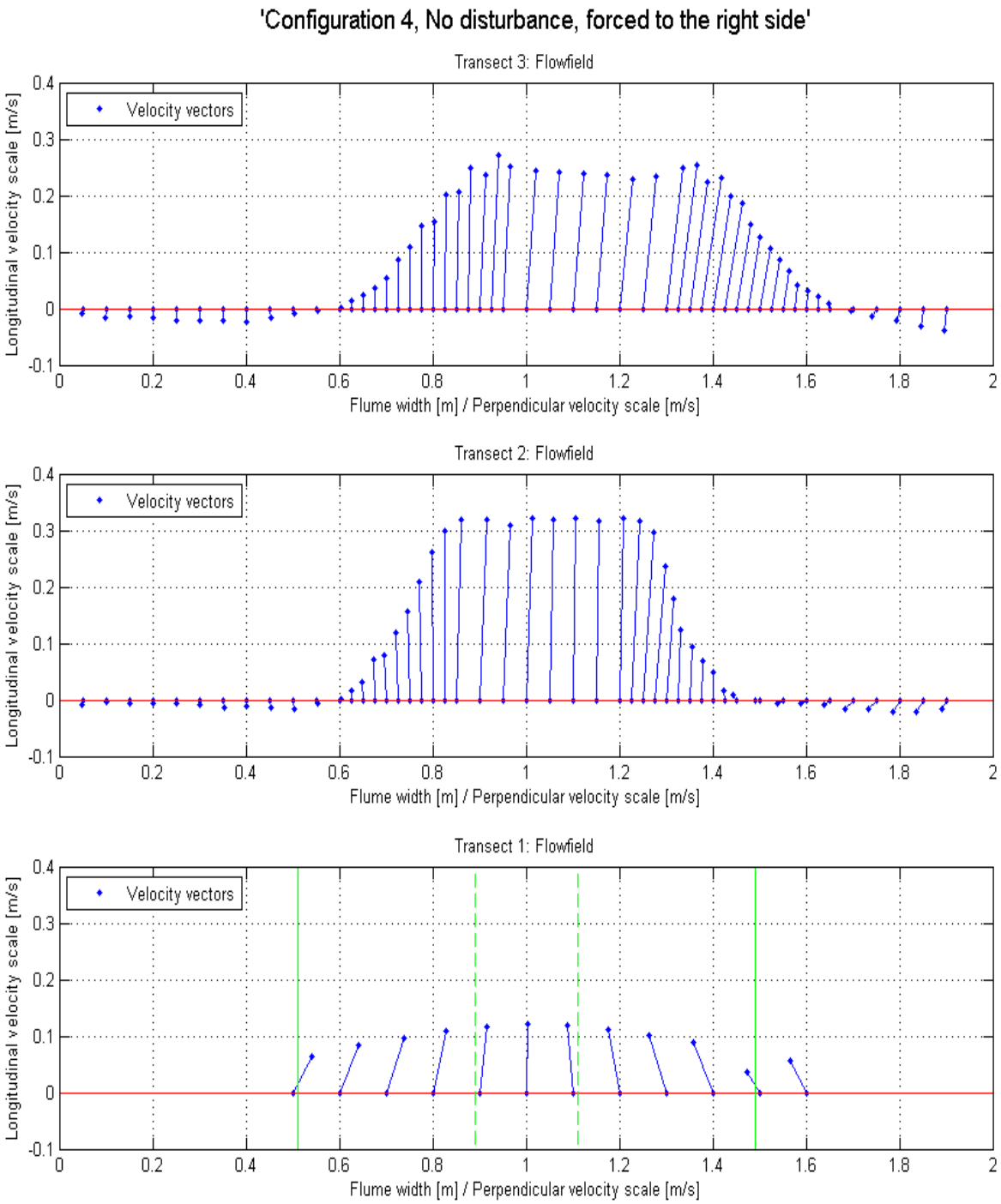
'Configuration 4, No disturbance, forced to the right side'
Transect 3: Flowfield
Velocity vectors
Longitudinal velocity scale [m/s]
Flume width [m] / Perpendicular velocity scale [m/s]
Transect 2: Flowfield
Velocity vectors
Longitudinal velocity scale [m/s]
Flume width [m] / Perpendicular velocity scale [m/s]
Transect 1: Flowfield
Velocity vectors
Longitudinal velocity scale [m/s]
Flume width [m] / Perpendicular velocity scale [m/s]

Appendix B: Power density spectrum